Nanoscale

Electrically Driven Structural Phase Transition in Single Ag_2Te Nanowire Devices

Journal:	*Nanoscale*
Manuscript ID	NR-ART-12-2018-010000.R1
Article Type:	Paper
Date Submitted by the Author:	27-Feb-2019
Complete List of Authors:	Premasiri, Kasun; Case Western Reserve University College of Arts and Sciences, Department of Physics Zheng, Wei; Iowa State University, Department of Chemical and Biological Engineering Xu, Biao; Iowa State University, Mechanical Engr. Ma, Tao; Ames Laboratory, U.S. Department of Energy Zhou, Lin; Ames National Lab, US Department of Eneygy Wu, Yue; Iowa State University, Department of Chemical and Biological Engineering; Gao, Xuan; Case Western Reserve University, Physics

Journal Name

ARTICLE

Electrically Driven Structural Phase Transition in Single Ag_2Te Nanowire Devices

Received 00th January 20xx,
Accepted 00th January 20xx

DOI: 10.1039/x0xx00000x

www.rsc.org/

Kasun Premasiri,[†a] Wei Zheng,[†b] Biao Xu,[b] Tao Ma,[c] Lin Zhou,[c] Yue Wu*[b] and Xuan P. A. Gao*[a]

Exploring new phase–change materials are instrumental in the progression of electronic memory devices. Ag_2Te with its reversible structural phase transition, and in the form of nanowires becomes an apt candidate to potentially use in nanoscale memory devices. Here we report a study on the temperature– or electrically–driven phase change properties of crystalline Ag_2Te nanowires. We first demonstrate that this structural phase change can be achieved via heating up the nanowires, which results in a sharp drop in conductance. Then we show that a DC voltage (< 1V) induced Joule heating can be used to reach the phase transition, even without any external heating. This work shows the potential of using Ag_2Te nanowires as a phase–change material in low voltage and low power nanoscale devices.

1. Introduction

The ceaseless demand for electronic memory in the evolution of electronics makes phase–change materials a constitutive facet of research in solid state physics and devices. In modern electronics, miniaturizing electronic memory devices[1-4] is becoming ever so important where nanostructures that can host phase changes draw a lot of attention mainly due to their unrivalled room for miniaturization. It has already been demonstrated that two–dimensional materials,[5-12] nanowires and nanoribbons[13-18] can be utilized as phase–change materials. Among different types of nanostructures, sub–lithographic dimensions combined with cylindrical shape add to the versatility of nanowires with structural phase changes as a potential class of materials for memory devices, specifically towards acquiring high storage density. However, utilizing nanowires as phase–change materials still largely remains as a less-explored territory, especially with the dearth of new reliable materials.

Germanium– and antimony–based tellurides serve as a benchmark for phase–change materials.[19-21] And Ag_2Te belongs to the family of silver chalcogenides which are known for their reversible structural phase transitions.[22] Ag_2Te is identified as Hessite in mineralogy.[23] This material has two distinct phases, namely α–Ag_2Te (cubic) and β–Ag_2Te (monoclinic).[24, 25] Ag_2Te possesses an antifluorite structure in its α form which transits to a distorted antifluorite structure as the material switches to β–Ag_2Te. Fig. 1a illustrates the atomic structure of β–Ag_2Te. Ag_2Te enters the α–phase from its β–phase above 417 K.[24] In its β form, Ag_2Te is a narrow bandgap semiconductor with a bandgap of a few tens of meV,[26] and has shown great promise as a thermoelectric material.[27, 28] Moreover, it has been demonstrated that β–Ag_2Te contains topological surface states.[29, 30]

There are various chemical and physical means such as pressure, temperature, chemical doping etc. that can be used to induce structural phase transitions. But most of those become incompetent in switching in memory devices either due to the inability to drive a phase transition reversibly and/or the necessity of extreme physical conditions that are unfavourable for applications. However, there are some materials that host structural phase transitions that can be triggered using a voltage. In this scenario, the voltage applied serves as an indirect way of bringing the required chemical or physical changes to trigger the phase change. There are basically two cases for which a voltage can be used to drive a phase change. Firstly, a voltage can be utilized to create an electric field via which strain can be applied to induce a pressure–driven phase change.[8, 31-33] Secondly, a voltage can be used to generate Joule heating that can trigger a temperature-driven phase change. These voltage-induced structural phase transitions provide ideal systems for switching, especially when the transition can be achieved within a reasonably low voltage (low energy consumption). In this work, we demonstrate the voltage–induced phase transition in Ag_2Te nanowires for the first time.

[a] *Department of Physics, Case Western Reserve University, Cleveland, OH 44106, USA.*
[b] *Department of Chemical and Biological Engineering, Iowa State University, Ames, IA 50011, USA.*
[c] *Division of Materials Science & Engineering, Ames Laboratory, U.S. DOE, Ames, IA 50011, USA.*
†Both authors contributed equally.
*Email: xuan.gao@case.edu (X.P.A.G.), yuewu@iastate.edu (Y.W.)
¶Electronic Supplementary Information (ESI) available: [details of any supplementary information available should be included here]. See DOI: 10.1039/x0xx00000x

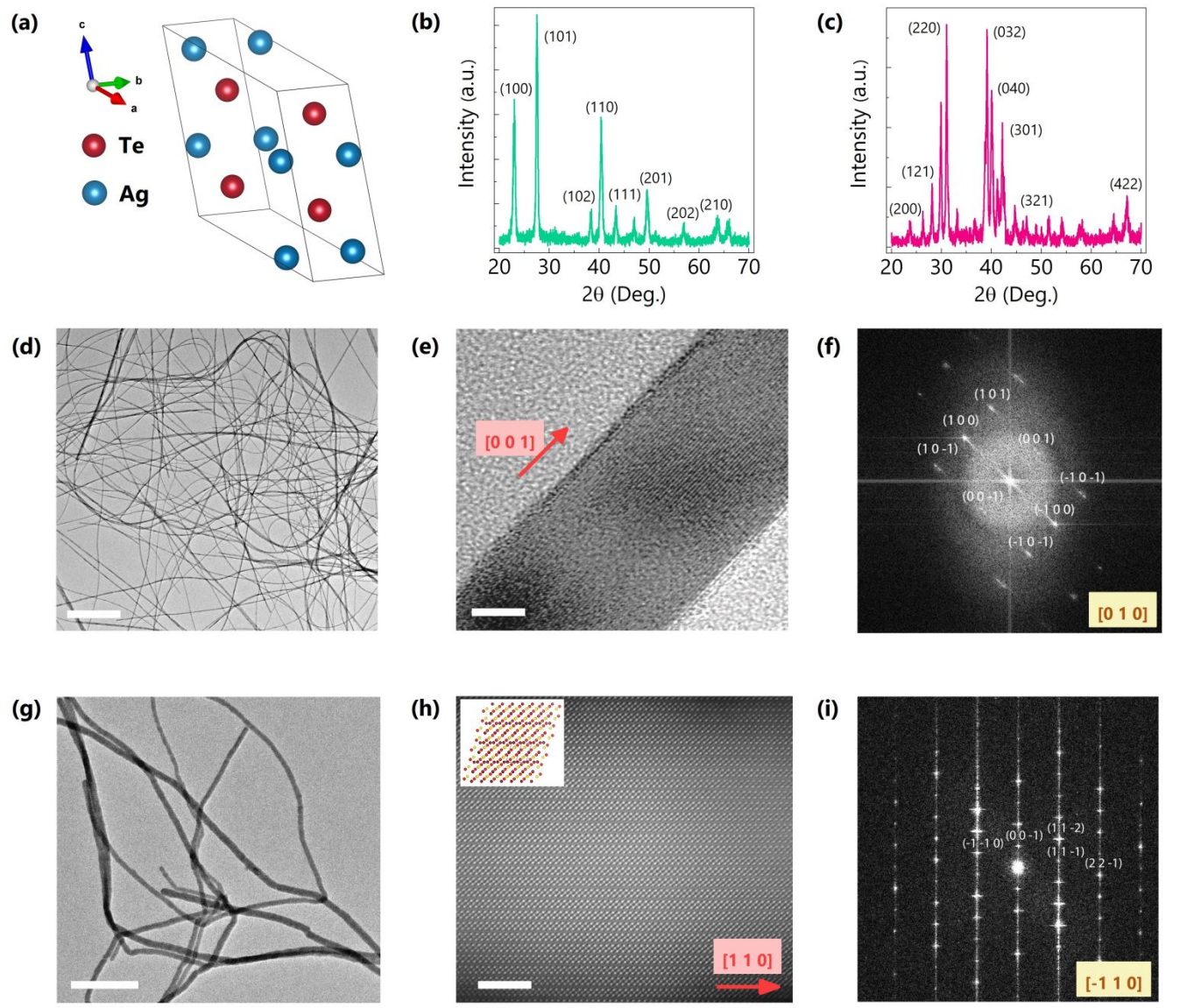

Fig. 1 (a) Schematic of the crystal structure of β–Ag_2Te. (b) An XRD analysis for Te nanowires. (c) An XRD analysis for Ag_2Te nanowires. (d) A TEM image of Te nanowires (scale bar: 500 nm). (e) An HRTEM image of Te nanowires (scale bar: 10 nm). (f) An FFT image of Te nanowires. The beam direction is [0 1 0]. (g) A TEM image of Ag_2Te nanowires (scale bar: 100 nm). (h) An STEM image of Ag_2Te nanowires (scale bar: 4 nm). Inset: The atomic structure (extended) of β–Ag_2Te to compare with the STEM. (i) An FFT image of Ag_2Te nanowires. The beam direction is [-1 1 0].

2. Experimental Section

2.1 Nanowire Synthesis

For this study, we use a solution-based synthesis route to obtain Ag_2Te nanowires. This kind of techniques has successfully been used elsewhere to synthesize various nanostructures.[34-37] Tellurium nanowires were synthesized first and then they were converted to Ag_2Te nanowires. For this, tellurium oxide (TeO_2, 99.99%) and silver nitrate ($AgNO_3$, 99.9%) were purchased from Alfa Aesar. Polyvinylpyrrolidone (PVP, with 40,000 g/ mol on average), potassium hydroxide (KOH, 99.99%), L-Ascorbic acid (99%), and hydrazine (anhydrous, 98%) were purchased from Sigma Aldrich. Ethylene glycol (EG) was purchased from VWR International.

***Tellurium Nanowires*:** 40.0 g of L-Ascorbic acid was dissolved in 120.0 ml of deionized water at 100 °C. Then, 6.4 g of TeO_2 (40 mmol), 20.0 g of PVP, 60.0 g of KOH and 600.0 ml of EG were added to a three-neck flask (1 L) and the temperature was set to 100 °C. Afterwards, the ascorbic acid solution was rapidly injected into the three-neck flask as the temperature reaches 100 °C. Then the system was allowed to react for 24 hours under nitrogen protection.

***Silver Telluride Nanowires*:** The as-synthesized tellurium nanowires

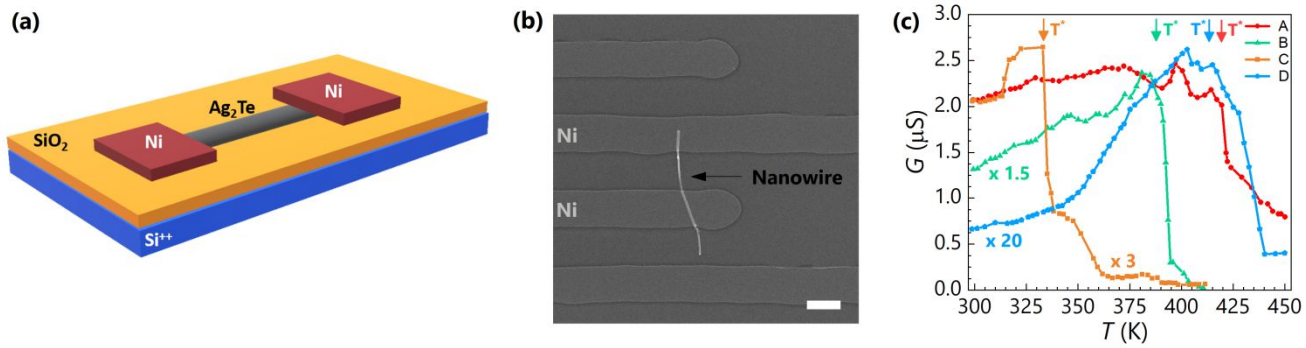

Fig. 2 (a) Schematic of the device structure of the Ag_2Te nanowire devices. (b) SEM image of a Ag_2Te nanowire device. Scale bar: 2 μm (white line). (c) Conductance vs temperature of single Ag_2Te nanowires (for Devices A, B, C and D) showing the transition at T^*.

were centrifuged three times with deionized water. Then, the tellurium nanowires were re-dispersed in 600.0 ml of EG. Alongside, 20.37 g of $AgNO_3$ (120 mmol) was added into 150.0 ml of EG, and then the mixture was dissolved with the aid of a sonicator, to prepare the silver precursor. Thereafter, the silver precursor was added dropwise to the tellurium nanowire solution and stirred at room temperature for an hour. This reaction converts tellurium into Ag_2Te. Then, the as-synthesized Ag_2Te nanowires was centrifuged two times with deionized water and washed in an ethanol solution (6% of hydrazine) for 2 hours. Then, they were washed twice with ethanol, and vacuum-dried. The transmission electron microscope (TEM) images in Fig. 1 show that the Te and Ag_2Te nanowires synthesized using this method are highly crystalline.

2.2 Device Fabrication

To demonstrate the structural phase change in individual nanowires, two-probe Ag_2Te nanowire devices were fabricated on Si (degenerately-doped) substrates with 300 nm thick silicon oxide on surface. At the onset, Si/SiO_2 substrates were sonicated in acetone for 20 min. Then they were rinsed with isopropyl alcohol followed by deionized water, and were blow-dried using compressed air. Afterwards, the cleaned SiO_2 surface was treated with ultraviolet-ozone at 150 °C for 10 min. Then, Ag_2Te nanowires (suspended in acetone) were drop-casted onto the cleaned SiO_2 surface. Thereafter, it was air-dried for a few min. A standard photolithography procedure (with a photomask of 2-micron minimum resolution) was used to pattern the SiO_2 surface with Ag_2Te nanowires embedded in the photoresist. Then the patterned chip was etched using an HF solution (1%) for 5 secs before depositing metal. This was to remove any possible native oxide that can build up on the surface of the Ag_2Te nanowires during the fabrication process. Removing the native oxide can help having good electrical contacts between the contact metal and the nanowire surface. Ni (60 nm) was evaporated (using an electron beam evaporator, Angstrom Evovac Deposition System). Afterwards, a standard photoresist remover was used to clear away the photoresist residue. Fig. 2a is a schematic of the device structure fabricated. All the devices used in this study had single nanowires confined between two Ni electrodes so that those two metal contacts can be used to apply a voltage across the nanowire. Moreover, the devices used for the study had Ohmic contacts, and thus additional annealing was not required. Fig. 2b is a scanning electron microscopy (SEM) image of one of the devices used in this study (Ni electrodes across which a voltage is applied are labeled).

2.3 Electrical Measurements

A probe station (Lakeshore) was utilized for the electrical measurements. Heating up the nanowires was carried out using the probe station's stage heater with the aid of a temperature controller (Lakeshore 332 Temperature Controller). Standard DC–techniques were used to obtain current–voltage (IV) and resistance measurements for the nanowires.

3. Results and Discussion

Fig. 1b and c show X-ray diffraction (XRD) analysis for Te and Ag_2Te nanowires, respectively. This analysis clearly shows all the signature peaks corresponding to Te and Ag_2Te crystallographic phases suggesting that the synthesized Ag_2Te is highly crystalline and pure. According to these results, Te nanowires can be indexed as in hexagonal phase (space group: 152; $P_{3(1)\,2\,1}$) and Ag_2Te nanowires can be indexed as in monoclinic phase (space group: 13; $P_{1\,2/c\,1}$). Fig. 1d and g are transmission electron microscopy (TEM) images of Te and Ag_2Te phases, respectively. Fig. 1e is a high-resolution transmission electron microscopy (HRTEM) image of a Te nanowire and the corresponding fast Fourier transform (FFT) image of it is shown as Fig. 1f. According to Fig. 1e, the growth direction for the Te nanowire is along [0 0 1] direction. Fig. 1h is a scanning transmission electron microscopy (STEM) image of an Ag_2Te nanowire. The inset of Fig. 1h illustrates the atomic structure (extended) of β–Ag_2Te to compare with the STEM analysis. The FFT image corresponding to the analysis in Fig. 1h is shown as Fig. 1i. *Moon et al* have shown that the [0 0 1]-oriented hexagonal Te transforms into [1 1 0]-oriented monoclinic phase. [25] This transformation is thermodynamically favorable. Therefore, the major growth directions for Te and Ag_2Te nanowires are [0 0 1] direction of Te and [1 1 0] direction of Ag_2Te, respectively. This confirms that the synthesized Ag_2Te nanowires are single crystal. However, since a solution phase method is utilized in synthesizing them, they may contain lattice defects. Furthermore, the energy-dispersive X-ray spectroscopy (EDS) mapping confirms a uniform distribution of Ag and Te in a large portion of a Ag_2Te nanowire (See ESI). According to this EDS analysis, the atomic ratio of Ag to Te is 66.14 to 33.86, and this confirms the stoichiometry of this phase of

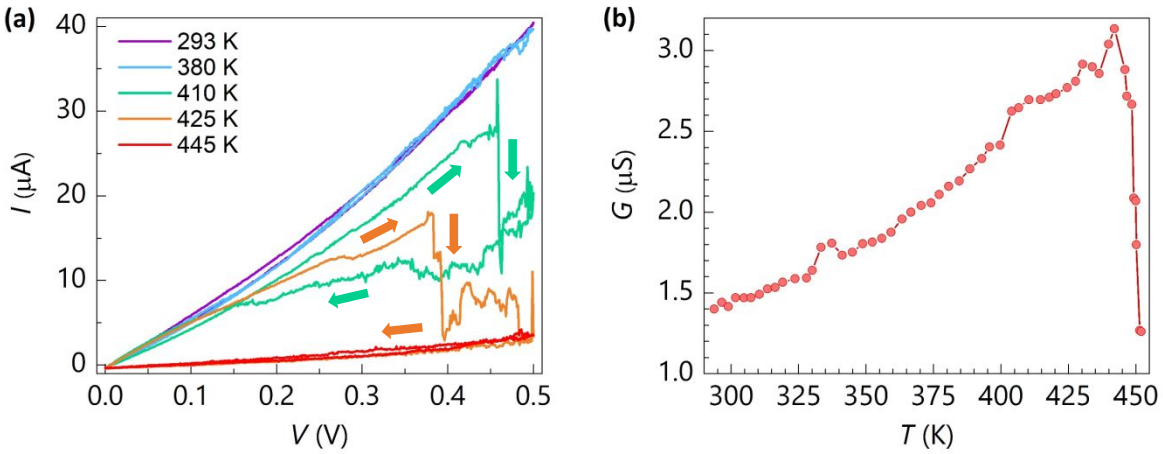

Fig. 3 (a) I vs V responses (for Device E) at different temperatures. The arrows are to indicate the direction of the loop. (b) Variation of conductance with temperature for Device E.

Ag_2Te as well.

The transition temperature (T_{tr}) between α and β phases of bulk Ag_2Te is 150 ◦C or 423 K ± 10K.[24] Fig. 2c shows the change in conductance with temperature for four different nanowire devices (Device A, B, C and D). *T** denotes the temperature reading of the sample stage of the probe station at the transition between α and β phases of Ag_2Te. Conductance values in Fig. 2c were extracted from I vs V measurements (within ± 100 mV), and all those devices showed linear IV responses (ESI Fig. S1.¶). Since a small voltage interval of mere ± 100 mV was used, the contribution from Joule heating to the conductance changes in Fig. 2c is negligible compared to the ambient temperature raising. In this series of experiments, all the devices exhibited conductance drop around the α to β phase transition temperature of Ag_2Te. However, the transition for Device A and Device D happened at temperatures close to the predicted value for the transition temperature (T_{tr}) in bulk Ag_2Te, while Device B and Device C showed transitions at temperatures lower than the bulk value. These variations are presumably due to the structural distinctions and/or irregularities in individual nanowires (e.g. diameter, lattice defects and etc.). More importantly, all four devices in Fig. 2c show sharp and significant changes in conductance near T^*, which are indicative of the phase change from conductive β phase to more resistive α phase Ag_2Te.[24] SEM images were acquired for all the devices in Fig. 2C. Diameters of the Ag_2Te nanowires of Device A, B, C and D can be approximated to be 200 nm, 250 nm, 150 nm and 150 nm, respectively. Hence, there is no any obvious correlation between T^* and the diameter of the nanowire.

In the aforementioned analysis (in Fig. 2c), the phase transition is triggered via elevating the temperature of the nanowire by heating up the surroundings. Joule heating can be used for the same purpose when the transition temperature for the phase transition is reasonably low. In this scenario, a voltage applied to the nanowire can be used to generate the required Joule heating. So the contributions from both the Joule heating and the ambient heating can be quantified as follows.

$$\Delta \boldsymbol{Q} = \Delta \boldsymbol{Q_T} + \Delta \boldsymbol{Q_J} \quad (1)$$

where, $\Delta \boldsymbol{Q}$ is the total thermal energy required to surpass the phase transition temperature, $\Delta \boldsymbol{Q_T}$ is the thermal energy supplied by the surroundings to heat up the nanowire and $\Delta \boldsymbol{Q_J}$ is the thermal energy provided via Joule self-heating. In Fig. 2c, the contribution from Joule heating was nullified ($\Delta \boldsymbol{Q_J} \sim \boldsymbol{0}$) by confining the maximum applied voltage to a very small value so that the elevation

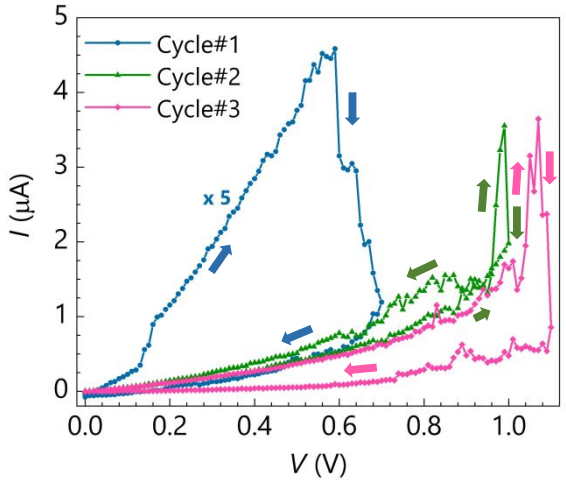

of the temperature of the nanowire is almost due to the heating of the surroundings.

Fig. 4 IV responses (Device F) at 296 K over multiple voltage loops.

Equivalent to the situation in Fig. 2c, one can supply the energy to heat up the nanowire via self–Joule–heating ($\Delta \boldsymbol{Q_J} > \boldsymbol{0}$). This becomes more convenient in controlling the phase change via a voltage applied across the nanowire, without the need to adjust the temperature of the environment; which can be very favourable in memory applications. The amount of Joule heating necessary to self-heat the nanowire above the transition temperature is proportional to the temperature difference between the transition temperature for the nanowire (T^*) and the ambient temperature, the specific heat of Ag_2Te, and the thermal conductance between the nanowire and the surroundings. Therefore, it is straightforward

to see that the higher the ambient temperature of the nanowire is, the lesser the Joule heating power necessary to induce the phase transition. This scenario is studied as the next step of this study (Fig. 3). For the IV curves in Fig. 3a, the ambient temperature of the nanowire and the maximum contribution from Joule heating are fixed, via fixing the temperature of the stage ($\boldsymbol{T}$) and the maximum voltage applied (0.5 V), respectively (Device E shows a linear IV response, ESI Fig. S3.¶). Moreover, the voltage sweeping rate was the same across all the IV responses in Fig. 3a (0.1 V/s). As illustrated in Fig. 3a, the $\Delta \boldsymbol{Q_J}$ provided by 0.5 V at both $\boldsymbol{T}$= 293 and 380 K is not large enough to trigger the phase transition. This suggests that a higher voltage (> 0.5 V) is required to induce the phase change in the region up to 380 K. As $\boldsymbol{T}$ is raised, the voltage corresponding to the required $\Delta \boldsymbol{Q_J}$ drops below 0.5 V. According to Fig. 3a, this happens within the region of $\boldsymbol{T}$= 380 - 410 K. And the phase transition is triggered around 0.45 V at 410 K. Further elevating the temperature brings the required voltage sequentially down, and eventually becomes zero leading to the condition $\boldsymbol{T^* - T = 0}$ which happens somewhere between 425 K to 445 K. Fig. 3b depicts the response of the conductivity of Device E to the temperature of the stage ($\boldsymbol{T}$) measured at low bias voltage ($\pm$ 100 mV), and it validates the T^* inferred in the voltage–driven phase transition in Fig. 3a.

This structural phase transition in Ag_2Te becomes more appealing in memory devices' perspective if it can be induced at room temperature over multiple cycles with the mere aid of a voltage. This aspect of Ag_2Te nanowire devices is studied and illustrated in Fig. 4, in which the phase transition is electrically-induced at room temperature over three times (Device F shows a linear IV response, ESI Fig. S4.¶). However, one important trend in Fig. 4 is that as more and more cycles are executed, the voltage required to surpass the phase change goes up in those subsequent cycles (Cycle#2 and Cycle#3 in Fig. 4 compared to Cycle#1) and the conductance at low bias voltage drops sequentially with the cycles (with Cycle#1 being the highest) (additional devices are illustrated in ESI¶). This reduced conductance means the voltage required to impart the same power ($\boldsymbol{P = V^2/R}$) increases for the subsequent cycles. But this trend of degrading conductance is not that obvious in Fig. 3a. Compared to the IV responses in Fig. 3a, larger voltages are used in Fig. 4. And also the voltage loops are run one after another without any lapse in between whereas in Fig. 3a, there is a relatively significant time interval between adjacent voltage loops due to the time it takes to heat up the nanowires using the stage heater. This suggests that the reduced conductance over continuous cycles in Fig. 4 could be due to irreversible degradations in the contacts of the device or the structure of the Ag_2Te nanowire. Such degradations in the contacts or the nanowire itself that require long recovery time might be due to the mismatch between Ag_2Te and Ni in thermal and mechanical properties or new lattice defects and grain boundaries generated temporarily during the phase transition process. Further enhancement to the device structure is necessary to minimize this effect so that better stability and durability can be achieved.

4. Conclusions

This study shows that resistive switching of individual Ag_2Te nanowires due to the structural phase transition between α–Ag_2Te and β–Ag_2Te can be driven by either direct thermal heating or indirect Joule heating via an electrical voltage bias of less than one volt. This study covers the vital aspects of the properties of the structural phase change of Ag_2Te, and also opens up the opportunity for further development of electrically controlled Ag_2Te nanowire phase change devices (e.g. inducing the phase change via a voltage pulse for high frequency applications).

Conflicts of interest

There are no conflicts to declare.

Acknowledgements

X. P. A. G. thanks the National Science Foundation (DMR-1151534) for its financial support. Y.W. thanks the support from the Office of Naval Research (N00014-16-1-2066).

References

1 P. S. Peercy, *Nature*, 2000, **406**, 1023-1026.
2 A. I. Kingon, J.-P. Maria and S. K. Streiffer, *Nature*, 2000, **406**, 1032-1038.
3 M. H. Devoret and R. J. Schoelkopf, *Nature*, 2000, **406**, 1039-1046.
4 S. Lloyd, *Nature*, 2000, **406**, 1047-1054.
5 Y. Wang, J. Xiao, H. Zhu, Y. Li, Y. Alsaid, K. Y. Fong, Y. Zhou, S. Wang, W. Shi, Y. Wang, A. Zettl, E. J. Reed and X. Zhang, *Nature*, 2017, **550**, 487-491.
6 D. H. Keum, S. Cho, J. H. Kim, D.-H. Choe, H.-J. Sung, M. Kan, H. Kang, J.-Y. Hwang, S. W. Kim, H. Yang, K. J. Chang and Y. H. Lee, *Nat. Phys.*, 2015, **11**, 482–486.
7 R. Kappera, D. Voiry, S. E. Yalcin, B. Branch, G. Gupta, A. D. Mohite and M. Chhowalla, *Nat. Mater.*, 2014, **13**, 1128–1134.
8 X. Qian, J. Liu, L. Fu and J. Li, *Science*, 2014, **346**, 1344-1347.
9 Y. Ma, L. Kou, X. Li, Y. Dai, S. C. Smith and T. Heine, *Phys. Rev. B*, 2015, **92**, 085427.
10 X. Xi, H. Berger, L. Forró, J. Shan and K. F. Mak, *Phys. Rev. Lett.*, 2016, **117**, 106801.
11 M. Yoshida, R. Suzuki, Y. Zhang, M. Nakano and Y. Iwasa, *Sci. Adv.*, 2015, **1**, e1500606.
12 J. Berry, S. Zhou, J. Han, D. J. Srolovitz and M. P. Haataja, *Nano Lett.*, 2017, **17**, 2473-2481.
13 S.-W. Nam, H.-S. Chung, Y. C. Lo, L. Qi, J. Li, Y. Lu, A. T. C. Johnson, Y. Jung, P. Nukala and R. Agarwal, *Science*, 2012, **336**, 1561-1566.
14 S.-H. Lee, Y. Jung and R. Agarwal, *Nat. Nanotechnol.*, 2007, **2**, 626-630.
15 P. Nukala, C.-C. Lin, R. Composto and R. Agarwal, *Nat. Commun.*, 2016, **7**, 10482.
16 F. Xiong, A. D. Liao, D. Estrada and E. Pop, *Science*, 2011, **332**, 568-570.
17 B. Jin, D. Kang, J. Kim, M. Meyyappan and J. Lee, *J. Appl. Phys.*, 2013, **113**, 164303.
18 F. F. Baldis, M. Sirena, L. B. Steren, V. H. Etgens, M. Eddrief, C. Ulysse and G. Faini, *Appl. Phys. Lett.*, 2015, **107**, 012407.
19 B.-S. Lee, J. R. Abelson, S. G. Bishop, D.-H. Kang, B.-K. Cheong and K.-B. Kim, *J. Appl. Phys.*, 2005, **97**, 093509.
20 S. Hudgens and B. Johnson, *MRS Bull.*, 2004, **29**, 829–832.

21 S. Raoux, F. Xiong, M. Wuttig and E. Pop, *MRS Bull.*, 2014, **39**, 703–710.
22 C. Xiao, J. Xu, K. Li, J. Feng, J. Yang and Y. Xie, *J. Am. Chem. Soc.*, 2012, **134**, 4287-4293.
23 Mineralogy Database, http://webmineral.com/data/Hessite.shtml#.W5avT-hKhPY (accessed September 2018)
24 F. Li, C. Hu, Y. Xiong, B. Wan, W. Yan and M. Zhang, *J. Phys. Chem. C*, 2008, **112**, 16130–16133.
25 G. D. Moon, S. Ko, Y. Xia and U. Jeong, *ACS Nano*, 2010, **4**, 2307–2319.
26 R. Dalven, *Phys. Rev. Lett.*, 1966, **16**, 311-312.
27 Y. Pei, N. A. Heinz and G. J. Snyder, *J. Mater. Chem.*, 2011, **21**, 18256.
28 H. Yang, J.-H. Bahk, T. Day, A. M. S. Mohammed, B. Min, G. J. Snyder, A. Shakouri and Y. Wu, *Nano Lett.*, 2014, **14**, 5398–5404.
29 S. Lee, J. In, Y. Yoo, Y. Jo, Y. C. Park, H.-J. Kim, H. C. Koo, J. Kim, B. Kim and K. L. Wang, *Nano Lett.*, 2012, **12**, 4194–4199.
30 W. Zhang, R. Yu, W. Feng, Y. Yao, H. Weng, X. Dai and Z. Fang, *Phys. Rev. Lett.*, 2011, **106**, 156808.
31 K.-A. N. Duerloo, Y. Li and E. J. Reed, *Nat. Commun.*, 2014, **5**, 4214.
32 S. Song, D. H. Keum, S. Cho, D. Perello, Y. Kim and Y. H. Lee, *Nano Lett.*, 2015, **16**, 188–193.
33 D. A. Rehn, Y. Li, E. Pop and E. J. Reed, *npj Comput. Mater.*, 2018, **4**, 2.
34 L. Yi, Y. Liu, N. Yang, Z. Tang, H. Zhao, G. Ma, Z. Su and D. Wang, *Energy Environ. Sci.*, 2013, **6**, 835.
35 L. Yi, D. Wang and M. Gao, *CrystEngComm*, 2012, **14**, 401–404.
36 Z. Li, X. Lai, H. Wang, D. Mao, C. Xing and D. Wang, *Nanotechnology*, 2009, **20**, 245603.
37 Y. Zheng, Y. Luo, C. Du, B. Zhu, Q. Liang, H. H. Hng, K. Hippalgaonkar, J. Xu and Q. Yan, *Mater. Chem. Front.*, 2017, **1**, 2457–2473.